MODELING OF SILICON QUANTUM STRUCTURES

University of Massachusetts - Boston

Gregory Sun

**AIR FORCE RESEARCH LABORATORY
SENSORS DIRECTORATE
ROME RESEARCH SITE
ROME, NEW YORK**
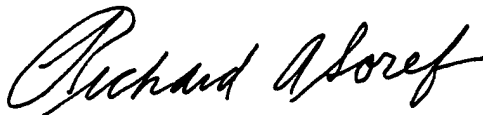
19990524 060

This report has been reviewed by the Air Force Research Laboratory, Information Directorate, Public Affairs Office (IFOIPA) and is releasable to the National Technical Information Service (NTIS). At NTIS it will be releasable to the general public, including foreign nations.
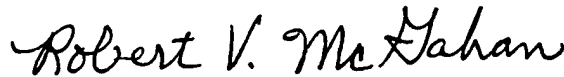
AFRL-SN-RS-TR-1999-65 has been reviewed and is approved for publication.

APPROVED: *Richard A Soref*

RICHARD A. SOREF
Project Engineer

FOR THE DIRECTOR: *Robert V. McGahan*

ROBERT V. McGAHAN, Technical Advisor
Electromagnetics Technology Division
Sensors Directorate

If your address has changed or if you wish to be removed from the Air Force Research Laboratory Rome Research Site mailing list, or if the addressee is no longer employed by your organization, please notify AFRL/SNHC, 80 Scott Drive, Hanscom AFB, MA 01731-2909. This will assist us in maintaining a current mailing list.

Do not return copies of this report unless contractual obligations or notices on a specific document require that it be returned.

REPORT DOCUMENTATION PAGE			*Form Approved* *OMB No. 0704-0188*

Public reporting burden for this collection of information is estimated to average 1 hour per response, including the time for reviewing instructions, searching existing data sources, gathering and maintaining the data needed, and completing and reviewing the collection of information. Send comments regarding this burden estimate or any other aspect of this collection of information, including suggestions for reducing this burden, to Washington Headquarters Services, Directorate for Information Operations and Reports, 1215 Jefferson Davis Highway, Suite 1204, Arlington, VA 22202-4302, and to the Office of Management and Budget, Paperwork Reduction Project (0704-0188), Washington, DC 20503.

1. AGENCY USE ONLY *(Leave blank)*	2. REPORT DATE April 1999	3. REPORT TYPE AND DATES COVERED Final Aug 97 - Aug 98	

4. TITLE AND SUBTITLE MODELING OF SILICON QUANTUM STRUCTURES	5. FUNDING NUMBERS C - F30602-97-2-0151 PE - 61102F PR - 2305
6. AUTHOR(S) Gregory Sun	TA - D2 WU - P5

7. PERFORMING ORGANIZATION NAME(S) AND ADDRESS(ES) University of Massachusetts - Boston 100 Morrissey Boulevard Boston MA 02125	8. PERFORMING ORGANIZATION REPORT NUMBER N/A

9. SPONSORING/MONITORING AGENCY NAME(S) AND ADDRESS(ES) Air Force Research Laboratory/SNHC 80 Scott Drive Hanscom AFB MA 01731-2909	10. SPONSORING/MONITORING AGENCY REPORT NUMBER AFRL-SN-RS-TR-1999-65

11. SUPPLEMENTARY NOTES

Air Force Research Laboratory Project Engineer: Richard A. Soref/SNHC/(781) 377-2380

12a. DISTRIBUTION AVAILABILITY STATEMENT Approved for public release; distribution unlimited.	12b. DISTRIBUTION CODE

13. ABSTRACT *(Maximum 200 words)*

The proposed research was to investigate the carrier optical-phonon interaction in a mixed polar-nonpolar material system of Si/ZnS superlattices, where not only carriers are confined, but also the optical phonons. The heavy-hole subbands and associated wave functions were calculated for Si/ZnS superlattices. Optical phonon confinement were modeled successfully using a continuum model with proper mechanical and electrostatic boundary conditions satisfied at the heterointerface. The established model for the confined optical phonons is used in calculating the intersubband heavy-hole scattering rate by optical phonons in the Si/ZnS superlattice. This work establishes the theoretical foundation to determine subband lifetimes in the design of Si/ZnS quantum well intersubband lasers.

14. SUBJECT TERMS Heavy-Hole Subbands, Si/ZnS Superlattices			15. NUMBER OF PAGES 28
			16. PRICE CODE

17. SECURITY CLASSIFICATION OF REPORT UNCLASSIFIED	18. SECURITY CLASSIFICATION OF THIS PAGE UNCLASSIFIED	19. SECURITY CLASSIFICATION OF ABSTRACT UNCLASSIFIED	20. LIMITATION OF ABSTRACT UL

Standard Form 298 (Rev. 2-89) (EG)
Prescribed by ANSI Std. 239.18
Designed using Perform Pro, WHS/DIOR, Oct 94

Executive Summary

The proposed research has been focused on the modeling of quantum processes in intersubband lasers of Si/ZnS superlattices, which could potentially offer the great opportunity for monolithic integration of Si-based photonic devices with advanced Si electronics. There are many new important and interesting quantum effects in this new mixed polar-nonpolar material system, arising from the fact that not only the carriers are confined, but also the polar and nonpolar optical phonons. So far, there has been little reported investigation on this material system. During the period of this research contract, we have calculated the valence subband engeries and wavefunctions in Si/ZnS quantum well structures. We have also established models for the confined optical phonons in Si/ZnS superlattices. Optical phonon modes in Si and ZnS layers are totally confined within their respective layers since both layers can be treated as infinitely rigid with respect to the other layer. Since there are no associated electric fields with nonpolar optical phonons in Si layers, only a mechanical boundary condition needs to be satisfied for these nonpolar optical modes at the Si-ZnS interface. The optical phonons in Si layers can be described by guided modes consisting of an uncoupled s-TO mode and a hybrid of LO and p-TO modes with no interface modes. In ZnS layers, a continuum model hybridizing the LO, TO and IP modes is necessary to satisfy both the mechanical and electrostatic boundary conditions at the heterointerface. A numerical procedure is provided to determine the common frequency between LO, TO, and IP modes. This is a new procedure for obtaining the eigen modes of a mixed polar-nonpolar heterosystem. Analytical expressions are obtained for the ionic displacement and associated electric field as well as scalar and vector potentials. The established optical-phonon model has then been used to calculate the phonon scattering process of heavy holes in Si/ZnS heterostructures. Our results indicate that contributions to the intersubband scattering rate from Si or ZnS confined optical phonons depend strongly on the distribution of envelope wave functions over the respective layers within which different types of optical phonons are confined. This work established a theoretical foundation for studying the lasing lifetimes of Si/ZnS intersubband lasers.

I. INTRODUCTION

The demonstration of the InGaAs/AlInAs intersubband quantum cascade laser at $\lambda = 4.2\mu m$[1, 2] has spurred interest in the use of silicon as the lasing material because of its integrability with advanced silicon microelectronics[3, 4]. There is also interest in moving the lasing from the far- and mid-infrared range to the near-infrared optical communications wavelengths, $\lambda = 1.3$ or $1.55\mu m$[5]. Since the latter wavelength corresponds to a photon energy of $800meV$, the $Si_{1-x}Ge_x$/Si heterosystem is inadequate because a maximum practical valence band offset of only $\sim 500meV$ can be obtained for pseudomorphic $Si_{1-x}Ge_x$ layers at $x = 0.5 \sim 0.6$. Therefore, alternative large-bandgap, nearly lattice-matched barrier materials for Si quantum wells must be sought; materials with sufficiently large band offsets with respect to silicon. Possible candidates include, ZnS, BeSeTe, CaF_2, SiO_x, SiO_2, the Si/SiO_2 superlattice, and γ-Al_2O_3, among others[5]-[7].

The Si/ZnS heterosystem has received the most attention as current advances in epitaxy technology have allowed the growth of heterostructures consisting of polar and nonpolar materials[8, 9]. The lattice mismatch of cubic ZnS with respect to Si is only 0.3%. The valence band offset has been predicted theoretically[10]-[13], while recent experiments[14] show that the value is close to $1.5eV$, sufficiently large to give intersubband energy differences in the desired $800meV$ range. MBE growth of ZnS upon Si, and Si upon ZnS have been demonstrated[9], with the use of an As monolayer to satisfy the local bonding requirements, although the effect of the monolayer on the offsets has not been determined.

The possibility of population inversion and the operation of intersubband lasers depend critically on the lifetimes of the involved subbands. The subband lifetimes in turn are determined by nonradiative phonon scattering processes. The purpose of the present paper is to study the optical phonon modes and their interaction with carriers in the Si/ZnS system since the optical phonon scattering is considered to be dominant in the phonon scattering processes. This combination of materials is new, since it consists of both a nonpolar and polar semiconductor. Previous studies in carrier scattering by confined optical phonons in heterostructures have been focused only on one type of phonons, either polar[15]-[23] or nonpolar[24]-[27]. In the current situation involving both polar and nonpolar materials, carrier scattering by both types of phonons needs to be considered. To the best of our knowledge, there has not been any reported investigation on this mixed nature of optical phonons, their confinement effect, and their interaction with carriers in a heterostructure. In this paper, we will present a theoretical study based on the macroscopic continuum model to describe the confined optical phonon modes and will use this model to calculate the optical-phonon scattering of heavy holes in a heterostructure consisting of polar (ZnS) and nonpolar materials (Si), as we are interested in the feasibility of constructing an intersubband laser within the valence band of the Si/ZnS heterostructure. This valence intersubband laser will likely be a quantum-parallel superlattice laser[28] or a quantum cascade laser. Our latest

thinking[29] is that each of the N laser periods will consists of one square Si quantum well containing two active heavy-hole subbands. Due to the non-parabolicity of these subbands, we believe that a population inversion, localized in k-space, can be engineered between the subbands. In this investigation, we will consider a simple superlattice comprised of alternating layers of Si and ZnS, much like the flat-band superlattice of the quantum parallel laser (Fig.2(b) of [28]). The results of this study will provide the basis for the calculation of subband lifetimes required to determine laser gain and threshold.

As described below in greater detail, since the optical dispersions (frequency versus wavevector) of the silicon ($\hbar\omega_{Si} = 64meV$) and zinc sulphide ($\hbar\omega_{ZnS} = 43meV$) have no overlap, the optical phonons are assumed to be totally confined in both materials. In the silicon layers, a continuum model with double hybridization of the longitudinal optical (LO) and transverse optical (TO) modes is used to describe the vibration patterns of the guided modes[24]. The only boundary condition that needs to be satisfied in the Si layers is the vanishing of the displacements at the Si-ZnS interface, since the ZnS layers can be considered as infinitely rigid with respect to the vibrations of the Si layer. Hence, there is no interface mode in the Si layers. The situation on the ZnS layers is more complex. Following the work by Ridley[16, 17], here a continuum model is employed with hybridization of the optical LO, TO, and interface polariton (IP) modes needed to satisfy both the mechanical and electrostatic boundary conditions at the interfaces. Specifically, the electrostatic boundary conditions are the continuity of E_x, the electric field parallel to the interface, and the continuity of D_z, the displacement field normal to the interface. The mechanical boundary condition is again the vanishing of the optical displacements since the Si layers can be considered as infinitely rigid with respect to the vibrations of the ZnS layers.

Our current work provides a complete set of analytical expressions for the optical phonon dispersion relations, optical displacements, and associated scalar and vector potentials. These expressions are subsequently used in calculating the interaction of heavy holes with the confined optical phonons. In Section II, we establish a continuum model for the optical displacement modes in Si and ZnS layers satisfying both mechanical and electrical boundary conditions. In section III, we outline a numerical procedure for determining the frequency of a ZnS optical mode inducing the intersubband scattering. In Section IV, we describe the scalar and vector potentials associated with the ZnS ionic displacement modes. In Section V, we calculate the intersubband scattering rate due to the emission of Si and ZnS optical phonons since the emission process is rather significant compared to the scattering process of optical phonon absorption. In Section VI, we summarize and discuss our results and conclusions.

II. Mode Patterns

A continuum model for the optical modes in the Si/ZnS superlattice is employed. Both mechanical and electrical boundary conditions are satisfied at the heterointerfaces. Since the optical dispersion relations (frequency versus phonon wavevector) in the two

4

bulk materials have no overlap, the phonons are taken to be confined in their respective materials. For the Si layers, the continuum model for optical phonons in nonpolar materials[24, 26] is used. Here double hybridization of the LO (longitudinal optical) and TO (transverse optical) modes is used to give the vibration patterns of the guided modes. Since the ZnS layers are infinitely rigid with respect to the vibrations of the Si layers, only the mechanical boundary condition, the vanishing of the displacements at the interfaces, has to be satisfied.

For the polar ZnS layers, the situation is more complex and an alternate continuum model[16, 17] consisting of an intermixing of confined LO, TO, and IP (interface polariton) modes is needed in order to satisfy both the electrostatic and mechanical boundary conditions. The boundary conditions which must be satisfied are (1) the continuity of E_x, the component of electric field parallel to the interface, (2) the continuity of D_z, the component of the displacement vector normal to the interface, and (3) the vanishing of the vector displacement u at the interface.

A. Modes in Si Layers

As discussed above, since the ZnS layers can be treated as infinitely rigid, the boundary condition to be satisfied in the Si layers is the vanishing of the ionic displacement of all confined vibration modes. This is an assumption of strict confinement yielding only the guided modes. As pointed out in the continuum theory[24], the ionic displacement of confined vibrations has two components: one is the hybrid of the LO and p-polarized TO (p-TO) modes, and other is the uncoupled s-polarized TO (s-TO) mode. These modes are defined as follows: If we consider a (x, z) plane containing the normal to the layers and the phonon wavevector $\mathbf{Q}$, then

$$\mathbf{Q} = q_x \hat{e}_x + q_z \hat{e}_z \tag{1}$$

where $\hat{e}_x$ and $\hat{e}_z$ are unit vectors. The p-TO mode has its displacements normal to $\mathbf{Q}$ and in the plane, while the s-TO displacements are normal to $\mathbf{Q}$ and perpendicular to the plane ($||\hat{e}_y$).

The form of the ionic displacement, scalar, and vector potentials in one superlattice period differs from that in a neighboring period only by a phase factor proportional to the Bloch superlattice wavevector q_{SL}. Their expressions given below are obtained by taking $q_{SL} = 0$. A description of the s-TO mode is

$$u_y = e^{iq_x x}(A_{s-TO} e^{iq_z z} + B_{s-TO} e^{-iq_z z}), \tag{2}$$

while the hybrid of the LO and p-TO modes is given by

$$
\begin{aligned}
u_x &= e^{iq_x x}[q_x(A_{LO} e^{iq_L z} + B_{LO} e^{-iq_L z}) + q_T(A_{p-TO} e^{iq_T z} + B_{p-TO} e^{-iq_T z})], \\
u_z &= e^{iq_x x}[q_L(A_{LO} e^{iq_L z} - B_{LO} e^{-iq_L z}) - q_x(A_{p-TO} e^{iq_T z} - B_{p-TO} e^{-iq_T z})],
\end{aligned}
\tag{3}
$$

which are confined within the Si layer with a width of d_{Si}, $0 < z < d_{Si}$. The z-components of the LO and TO wavevector have been distinguished by q_L and q_T, respectively.

Since the LO and TO modes must have the same frequency to be effectively coupled, we must satisfy the condition

$$\omega^2 = \omega_O^2 - \alpha_L^2(q_x^2 + q_L^2) = \omega_O^2 - \alpha_T^2(q_x^2 + q_T^2), \tag{4}$$

where ω_O is the bulk Si optical phonon frequency at Γ point, α_L and α_T are the sound velocities of LO and TO dispersions in Si, respectively.

Using the boundary condition that $\mathbf{u} = 0$ at the interfaces gives for the s-TO mode

$$u_y = Ae^{iq_x x}\sin(q_z z), \qquad \text{with} \quad q_z = \frac{n\pi}{d_{Si}} \tag{5}$$

where $n = 1, 2, \cdots$ and A is a mode coefficient. This mode does not mix with other modes.

The hybrid LO and p-TO modes admit two classes of solutions. The 'sine' solution is

$$\begin{aligned}
u_x &= 2Be^{iq_x x}q_x[\cos(q_L z) - \cos(q_T z)], \\
u_z &= 2iBe^{ik_x x}[q_L \sin(q_L z) + \frac{q_x^2}{q_T}\sin(q_T z)],
\end{aligned} \tag{6}$$

and the 'cosine' solution is

$$\begin{aligned}
u_x &= 2iBe^{iq_x x}[q_x \sin(q_L z) + \frac{q_L q_T}{q_x}\sin(q_T z)], \\
u_z &= 2Be^{iq_x x}q_L[\cos(q_L z) - \cos(q_T z)]
\end{aligned} \tag{7}$$

where

$$q_L = \frac{n_L \pi}{d_{Si}} \quad \text{and} \quad q_T = \frac{n_T \pi}{d_{Si}}, \tag{8}$$

where $n_L = 1, 2, \cdots$, $n_T = 3, 4, \cdots$, $n_T - n_L = 2, 4, 6, \cdots$, and B is a mode coefficient. No interface modes exist in the Si layer because of the boundary condition $\mathbf{u} = 0$.

The lowest s-TO mode pattern in Eq.(5) for $q_z = \pi/d_{Si}$ is shown in Fig.1(a) within a Si layer of $d_{Si} = 40\text{Å}$, while the hybrid patterns of the lowest p-TO and LO modes with $q_L = \pi/d_{Si}$ and $q_T = 3\pi/d_{Si}$ are shown in Figs.1(b) and 1(c) for the 'sine' and 'cosine' solutions given in Eqs.(6) and (7), respectively within the same Si layer. The strict confinement which requires the vanishing of ionic displacements at the boundaries

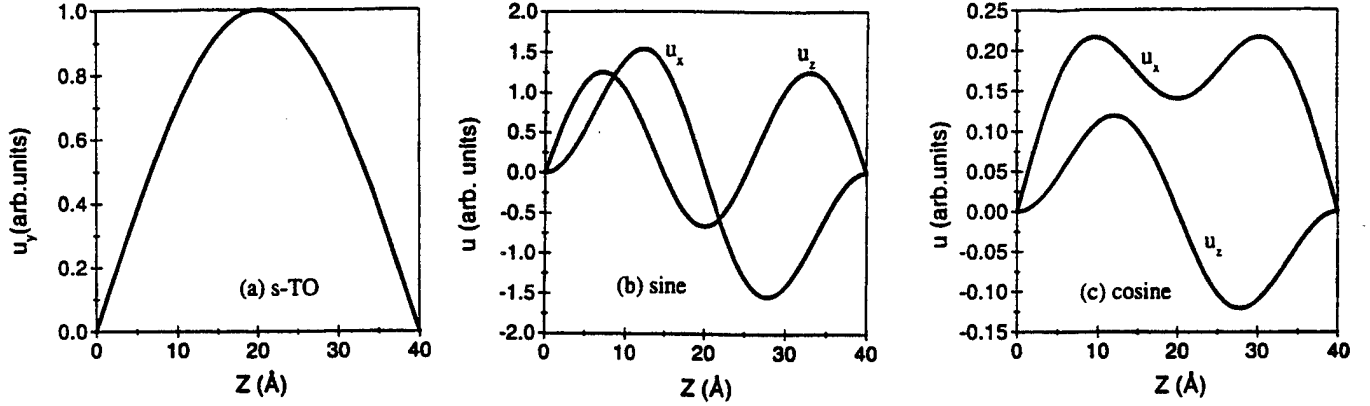of Si layers is clearly demonstrated for both vibration modes.

Figure 1. Vibration patterns in a Si layer with a width of 40$\mathring{A}$ for (a) the guided s-TO mode, (b) the 'sine' solution, and (c) the 'cosine' solution of the guided p-TO and LO modes.

B. Modes in ZnS Layers

The boundary conditions are the continuity of E_x, D_z, and the vanishing of **u** at the interfaces. These conditions can be satisfied by a unique linear combination of LO, TO, and IP modes with common frequency and common in-plane wavevector q_x,

$$\mathbf{u} = \mathbf{u}_{LO} + \mathbf{u}_{TO} + \mathbf{u}_{IP}. \tag{9}$$

We will use this hybrid expression to calculate the electrical interaction with carriers which is considerably stronger than the optical deformation potential interaction. We need consider only the displacements u_x and u_z, since u_y associated with the s-TO mode has no related electric field and therefore does not interact with carriers electrically. Once again, the expressions are obtained by taking the Bloch superlattice wavevector $q_{SL} = 0$.

For the LO mode, the ionic displacements are

$$
\begin{aligned}
u_x &= e^{i(q_x x - \omega t)} q_x (A_L e^{iq_L z} + B_L e^{-iq_L z}), \\
u_z &= e^{i(q_x x - \omega t)} q_L (A_L e^{iq_L z} - B_L e^{-iq_L z}).
\end{aligned}
\tag{10}
$$

which is confined within the ZnS layer with a width of d_{ZnS}, $-d_{ZnS}/2 < z < d_{ZnS}/2$

The associated electric fields are

$$E_x = -\rho_o u_x, \qquad E_z = -\rho_o u_z, \tag{11}$$

where

$$\rho_o = \frac{e^*}{\epsilon_o \Omega}, \tag{12}$$

7

with the effective ionic charge

$$e^{*2} = M\Omega\omega_{LO}^2\epsilon_o^2\left(\frac{1}{\epsilon_\infty} - \frac{1}{\epsilon_s}\right),$$ (13)

where M is the reduced mass, ϵ_o is the permittivity of free space, ϵ_∞, ϵ_s are the high-frequency and static permittivities, and Ω is the volume of primitive unit cell. The scalar potential ϕ associated with the electric field $\mathbf{E} = -\nabla\phi$ is in turn given as

$$\phi = -i\rho_o e^{i(q_x x - \omega t)}(A_L e^{iq_L z} + B_L e^{-iq_L z}).$$ (14)

For the TO mode

$$u_x = e^{i(q_x x - \omega t)} q_T (A_T e^{iq_T z} + B_T e^{-iq_T z}),$$
$$u_z = -e^{i(q_x x - \omega t)} q_x (A_T e^{iq_T z} - B_T e^{-iq_T z}).$$ (15)

The electric fields associated with this mode are negligible.

For the IP mode

$$u_x = e^{i(q_x x - \omega t)} q_p (A_P e^{iq_p z} + B_P e^{-iq_p z}),$$
$$u_z = i e^{i(q_x x - \omega t)} q_p (A_P e^{iq_p z} - B_P e^{-iq_p z})$$ (16)

The associated electric fields are

$$E_x = -\rho_p u_x, \qquad E_z = -\rho_p u_z,$$ (17)

where

$$\rho_p = \rho_o \frac{\omega^2 - \omega_{TO}^2}{\omega_{LO}^2 - \omega_{TO}^2},$$ (18)

and ω_{LO} and ω_{TO} are bulk ZnS LO and TO optical phonon frequencies at Γ point, respectively. The electric fields associated with the interface modes propagate into the Si layers although they are treated as infinitely rigid and do not contain ZnS ionic displacement.

Being a transverse electromagnetic wave, there is a vector potential $\mathbf{A}$ associated with the electric field $\mathbf{E} = -\partial\mathbf{A}/\partial t$. Within the ZnS layers,

$$A_x = i\frac{\rho_p}{\omega} e^{i(q_x x - \omega t)} q_p (A_P e^{iq_p z} + B_P e^{-iq_p z});$$
$$A_z = -\frac{\rho_p}{\omega} e^{i(q_x x - \omega t)} q_p (A_P e^{iq_p z} - B_P e^{-iq_p z})$$ (19)

While in the Si layers, a similar expression can be obtained with another set of mode coefficients, A_{p1} and B_{p1}.

Since large in-plane wavevectors are likely to be involved when dealing with carrier transitions due to optical phonons between two subbands separated with a relatively large energy, we have endeavored to obtain analytical dispersions of the LO and TO

8

optical branches by curve-fitting the experimental bulk phonon dispersions for the entire Brillioun zone. The requirement for common frequency yields,

$$
\begin{aligned}
\omega &= \omega_{LO} - \beta_L(q_x^2 + q_L^2) \\
&= \omega_{TO} - \beta_T(q_x^2 + q_T^2) \\
&= \frac{c(q_x^2 + q_p^2)^{1/2}}{n(\omega)}
\end{aligned}
\tag{20}
$$

where $\beta_L = 0.808 THz \cdot \AA^2$ and $\beta_T = 2.194 THz \cdot \AA^2$ are obtained from curve-fitting the bulk ZnS optical phonon dispersions, c is the velocity of light in vacuum, and $n(\omega)$ is the index of refraction. In the above expressions, the frequency in the ZnS layers lies between the ZnS LO and TO zone center frequencies. Since $\omega_{TO} < \omega_{LO}$, in order for the TO frequency to be equal to a LO frequency q_T must be imaginary $q_T = iq_o$, corresponding to a TO interface mode. The modes which interact most strongly with carriers are those with frequencies near the LO branch. For these modes, the value of q_o is large, and we can take the approximation

$$
\tanh(q_o d_{ZnS}) \approx 1.
\tag{21}
$$

In the unretarded limit ($c \to \infty$), $q_x^2 + q_p^2 \approx 0$ for the IP mode. Hence, $q_p \approx iq_x$.

Applying, at the two interfaces between layers Si and ZnS in a period of the superlattice, the conditions that u_x and u_z equal to zero along with the continuity of E_x and D_z, leads to eight simultaneous equations involving the eight unknown mode coefficients ($A_L, B_L; A_T, B_T; A_P, B_P;$ and A_{P1}, B_{P1}). The following two ionic displacement mode patterns emerge for the hybrid in Eq.(9) taking the Bloch superlattice wavevector $q_{SL} = 0$ and the approximation $\tanh(q_o d_{ZnS}) \approx 1$. Both ionic displacement patterns are confined within the ZnS layer, $-d_{ZnS}/2 < z < d_{ZnS}/2$. For the first type,

$$
\begin{aligned}
u_x = {} & 2iBe^{iq_x x}q_x\{\sin(q_L z) \\
& -[1 - p_1 \tanh(q_x d_{ZnS}/2)]\sin(q_L d_{ZnS}/2)\frac{\sinh(q_o z)}{\sinh(q_o d_{ZnS}/2)} \\
& -p_1 \sin(q_L d_{ZnS}/2)\frac{\sinh(q_x z)}{\cosh(q_x d_{ZnS}/2)}\}, \\
u_z = {} & 2Be^{iq_x x}q_L\{\cos(q_L z) \\
& -\frac{q_x^2}{q_L q_o}[1 - p_1 \tanh(q_x d_{ZnS}/2)]\sin(q_L d_{ZnS}/2)\frac{\cosh(q_o z)}{\sinh(q_o d_{ZnS}/2)} \\
& -\frac{q_x}{q_L}p_1 \sin(q_L d_{ZnS}/2)\frac{\cosh(q_x z)}{\cosh(q_x d_{ZnS}/2)}\},
\end{aligned}
\tag{22}
$$

9

and for the second type,

$$
\begin{aligned}
u_x = \; & 2Be^{iq_x x}q_x\{\cos(q_L z) \\
& -[1 - p_2\coth(q_x d_{ZnS}/2)]\cos(q_L d_{ZnS}/2)\frac{\cosh(q_o z)}{\sinh(q_o d_{ZnS}/2)} \\
& -p_2\cos(q_L d_{ZnS}/2)\frac{\cosh(q_x z)}{\sinh(q_x d_{ZnS}/2)}\}, \\
u_z = \; & 2iBe^{iq_x x}q_L\{\sin(q_L z) \\
& +\frac{q_x^2}{q_L q_o}[1 - p_2\coth(q_x d_{ZnS}/2)]\cos(q_L d_{ZnS}/2)\frac{\sinh(q_o z)}{\sinh(q_o d_{ZnS}/2)} \\
& +\frac{q_x}{q_L}p_2\cos(q_L d_{ZnS}/2)\frac{\sinh(q_x z)}{\sinh(q_x d_{ZnS}/2)}\},
\end{aligned}
\tag{23}
$$

where

$$
\begin{aligned}
p_1 &= \frac{\cosh(q_x d_{Si}/2)\cosh(q_x d_{ZnS}/2)}{d}, \\
p_2 &= \frac{\sinh(q_x d_{Si}/2)\sinh(q_x d_{ZnS}/2)}{d}, \\
d &= r\sinh(q_x d_{Si}/2)\cosh(q_x d_{ZnS}/2) + \sinh(q_x d_{ZnS}/2)\cosh(q_x d_{Si}/2), \\
r &= \frac{\epsilon_{p1}}{\epsilon_{p2}},
\end{aligned}
\tag{24}
$$

and ϵ_{p1} and ϵ_{p2} are the permittivities in Si and ZnS layers, respectively, with

$$
\epsilon_{p2} = \epsilon_\infty \frac{\omega^2 - \omega_{LO}^2}{\omega^2 - \omega_{TO}^2}.
\tag{25}
$$

To illustrate the patterns of ionic displacements in the ZnS layers given in Eqs.(22) and (23), we need to first determine values for q_x, q_L, and q_o. To do so, we will follow the numerical procedure described in Section III by arbitrarily fixing a value for the in-plane phonon wavevector $q_x = \pi/(5a_{ZnS})$, where a_{ZnS} is the lattice constant of ZnS. In calculating the carrier-optical phonon interaction, the value of q_x is actually determined by the conservation of in-plane momentum between the initial and final states of the scattering process. For a given value of q_x, typically, a set of hybridized modes can be obtained. Here, we show only the mode pattern with frequency close to ω_{LO}.

We obtained $\hbar\omega = 41meV$, $q_L = 0.46 \times 10^8/cm$ and $q_o = 0.48 \times 10^8/cm$. Substituting these values into Eqs.(22) and (23), we obtained Figs.2(a) and 2(b) showing the mode patterns of ionic displacement of both the first and second types, respectively in a ZnS layer of $d_{ZnS} = 20\overset{\circ}{A}$. It can be seen from Figs.2(a) and 2(b) that the mechanical boundary condition, vanishing of the ionic displacements at the interfaces of Si and ZnS
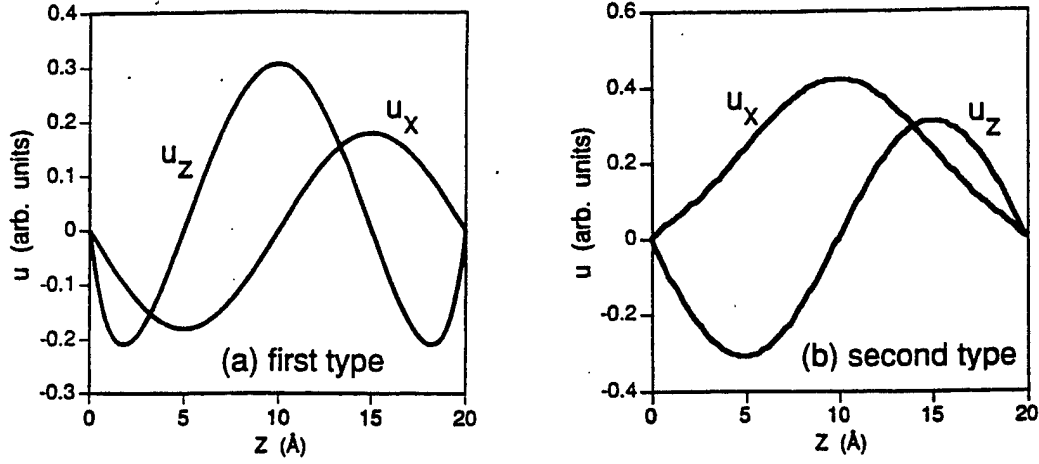
layers, is satisfied.

Figure 2. Vibration patterns in a ZnS layer with a width of $20\mathring{A}$ for (a) the first type and (b) the second type solutions of the hybridized LO, TO and IP modes.

III. Dispersion Relationship

The phonon frequency in the ZnS layers is determined by the following set of equations;

$$\left\{ \begin{array}{l} \omega = \omega_{LO} - \beta_L(q_x^2 + q_L^2), \\ \omega = \omega_{TO} - \beta_T(q_x^2 - q_o^2), \\ t_1 + t_2\cos(q_L d_{ZnS}) + t_3\sin(q_L d_{ZnS}) = 0 \end{array} \right. \tag{26}$$

where

$$\begin{array}{ll} t_1 = & 4p\sinh(q_x d_{Si}) + 4pr\sinh(q_x d_{ZnS}), \\ t_2 = & -4p\alpha, \\ t_3 = & 8p^2 r\sinh(q_x d_{ZnS})\sinh(q_x d_{Si}) - 4p^2\alpha^2 \\ & +4p^2 r^2\sinh^2(q_x d_{ZnS}) + 4p^2\sinh^2(q_x d_{Si}) + 1, \end{array} \tag{27}$$

with

$$p = \frac{q_x}{4q_L rsd} \tag{28}$$

and

$$s = \frac{\omega^2 - \omega_{TO}^2}{\omega_{LO}^2 - \omega_{TO}^2}. \tag{29}$$

The third equation in (26) is obtained from the requirement of a nonzero solution for the eight simultaneous equations discussed above, and Eq.(27) is arrived at under the approximation, $\tanh(q_o d_{ZnS}) \approx 1$.

The numerical procedure for determining a phonon frequency is the following: given a value of q_x, we can determine those of t_1, t_2, and t_3 from Eq.(27). Then ω is scanned from ω_{TO} to ω_{LO}. For a given value of ω, q_L and q_o are obtained from the first

two equations in (26). Those values are then substituted into the third equation in (26) to determine if the particular value of ω is a solution.

IV. Scalar and Vector Potentials

Associated with the two types of ionic displacement in Eqs.(22) and (23), the scalar potentials in ZnS layers are given as, for the first type,

$$
\phi = \begin{cases} 2\rho_o B e^{iq_x x} \sin(q_L z_1) & |z_1| < \dfrac{d_{ZnS}}{2} \quad \text{ZnS layer,} \\ 0 & |z_2| < \dfrac{d_{Si}}{2} \quad \text{Si layer,} \end{cases} \tag{30}
$$

and for the second type,

$$
\phi = \begin{cases} -2i\rho_o B e^{iq_x x} \cos(q_L z_1) & |z_1| < \dfrac{d_{ZnS}}{2} \quad \text{ZnS layer,} \\ 0 & |z_2| < \dfrac{d_{Si}}{2} \quad \text{Si layer.} \end{cases} \tag{31}
$$

Note that we have used two different coordinates z_1 and z_2 for layers ZnS and Si, respectively, with their origins placed at the centers of the respective layers.

The vector potentials can be obtained, for the first type,

$$
A_x = \begin{cases} \dfrac{2s\rho_o q_x}{\omega} B e^{iq_x x} p_1 \sin(q_L d_{ZnS}/2)\dfrac{\sinh(q_x z_1)}{\cosh(q_x d_{ZnS}/2)} & |z_1| < \dfrac{d_{ZnS}}{2} \quad \text{ZnS layer,} \\ \dfrac{4q_x\rho_o}{\omega} B e^{iq_x x} V_1 \sinh(q_x z_2) & |z_2| < \dfrac{d_{Si}}{2} \quad \text{Si layer,} \end{cases} \tag{32}
$$

$$
A_z = \begin{cases} \dfrac{2is\rho_o q_x}{\omega} B e^{iq_x x} p_1 \sin(q_L d_{ZnS}/2)\dfrac{\cosh(q_x z_1)}{\cosh(q_x d_{ZnS}/2)} & |z_1| < \dfrac{d_{ZnS}}{2} \quad \text{ZnS layer,} \\ \dfrac{4iq_x\rho_o}{\omega} B e^{iq_x x} V_1 \cosh(q_x z_2) & |z_2| < \dfrac{d_{Si}}{2} \quad \text{Si layer,} \end{cases} \tag{33}
$$

and for the second type,

$$
A_x = \begin{cases} -\dfrac{2is\rho_o q_x}{\omega} B e^{iq_x x} p_2 \cos(q_L d_{ZnS}/2)\dfrac{\cosh(q_x z_1)}{\sinh(q_x d_{ZnS}/2)} & |z_1| < \dfrac{d_{ZnS}}{2} \quad \text{ZnS layer,} \\ \dfrac{4iq_x\rho_o}{\omega} B e^{iq_x x} V_2 \cosh(q_x z_2) & |z_2| < \dfrac{d_{Si}}{2} \quad \text{Si layer,} \end{cases} \tag{34}
$$

$$
A_z = \begin{cases} -\dfrac{2s\rho_o q_x}{\omega} B e^{iq_x x} p_2 \cos(q_L d_{ZnS}/2)\dfrac{\sinh(q_x z_1)}{\sinh(q_x d_{ZnS}/2)} & |z_1| < \dfrac{d_{ZnS}}{2} \quad \text{ZnS layer,} \\ \dfrac{4q_x\rho_o}{\omega} B e^{iq_x x} V_2 \sinh(q_x z_2) & |z_2| < \dfrac{d_{Si}}{2} \quad \text{Si layer,} \end{cases} \tag{35}
$$

12

where

$$V_1 = \frac{r \sin(q_L d_{ZnS}/2) \cosh(q_x d_{ZnS}/2)}{2d},$$

$$V_2 = \frac{r \cos(q_L d_{ZnS}/2) \sinh(q_x d_{ZnS}/2)}{2d},$$

(36)

and p_1, p_2, and d are given in Eq.(24).

The scalar potentials associated with the LO modes are strictly confined within the ZnS layers. Their distributions are shown in Fig.3 for the first and second types given in Eqs.(30) and (31) with $q_L = 0.31 \times 10^8/cm$, $d_{ZnS} = 20\AA$, respectively.

The vector potential associated with the IP modes are distributed in both Si and ZnS layers, even though Si layers are treated as infinitely rigid and do not contain ZnS ionic displacements. The profiles for the two components of the vector potentials given in Eqs.(32-35) for the first and second types with $d_{Si} = 40\AA$, $d_{ZnS} = 20\AA$ are shown in Figs.4(a) and 4(b), respectively.
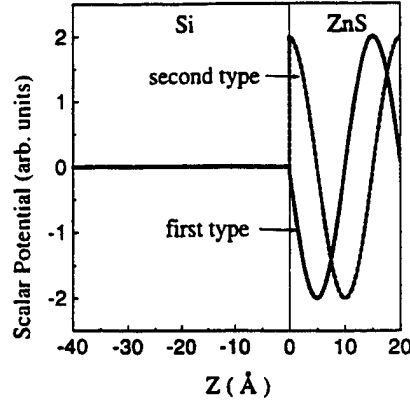

Figure 3. Scalar potential distribution associated with the LO modes in a period of the Si/ZnS superlattice with $d_{Si} = 40\AA$ and $d_{ZnS} = 20\AA$ for both the first and second types of the vibration modes.

It can be seen from Figs.3 and 4 that both scalar and vector potentials are not continuous across the interfaces. However, as pointed by Ridley[16], the energy of interaction with an electron traveling coherently with the optical phonon is continuous. The electric field can be obtained as

$$\mathbf{E} = -\nabla\phi - \frac{\partial \mathbf{A}}{\partial t}.$$

(37)

The continuity of E_x and $D_z = \epsilon(\omega)E_z$ implies that at the boundaries,

$$\omega A_x|_{z_2=\pm d_{Si}/2} = -q_x\phi|_{z_1=\mp d_{ZnS}/2} + \omega A_x|_{z_1=\mp d_{ZnS}/2},$$

$$A_z|_{z_2=\pm d_{Si}/2} = r A_z|_{z_1=\mp d_{ZnS}/2},$$

(38)

13

where A_{1x} and A_{1z} are x- and z-components of the vector potential in Si layers. The interaction in the Si layer is $e(A_{1x}v_x + A_{1z}v_z)$ and in the ZnS layer $e(-\phi + A_x v_x + A_z v_z)$, which are equal when the electron velocity $v_x = \omega/q_x$ and $v_z = 0$. Thus, the coherent interaction energy is continuous across the interfaces.
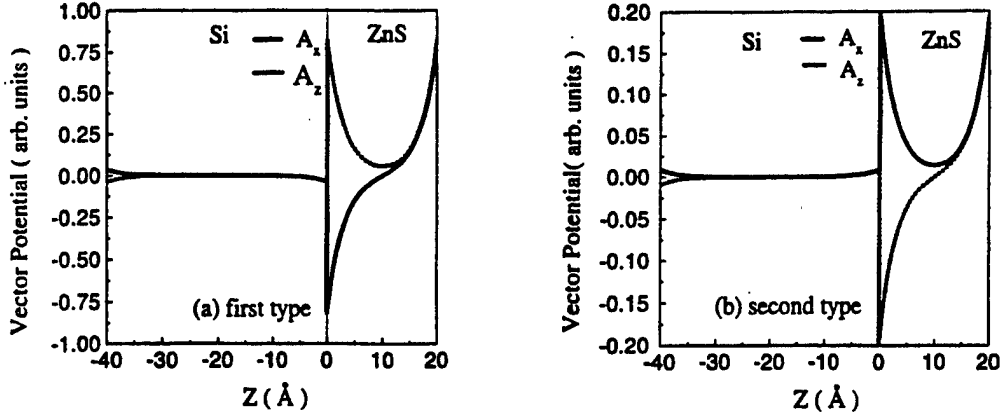

Figure 4. Vector potentials associated with the IP modes distributed in a period of the Si/ZnS superlattice with $d_{Si} = 40\mathring{A}$ and $d_{ZnS} = 20\mathring{A}$ for (a) the first type and (b) the second type of the vibration modes.

The electric field distributions for E_x and $\epsilon(\omega)$ in Si $(d_{Si} = 40\mathring{A})$ and ZnS $(d_{ZnS} = 40\mathring{A})$ layers are shown in Figs.5(a) and 5(b) for the first and second types, respectively. The continuity of E_x and D_z across the Si and ZnS interface according to Eq.(38) is clearly demonstrated.
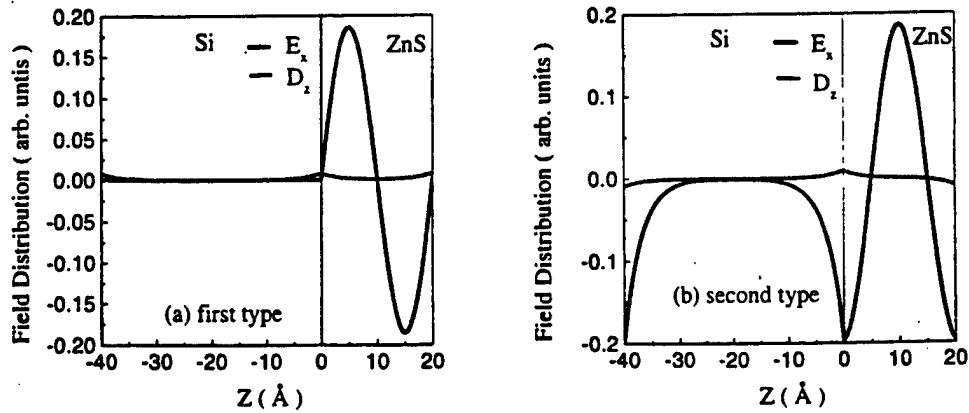

Figure 5. The field distributions, E_x and D_z, derived from the scalar and vector potentials, in a period of the Si/ZnS superlattice with $d_{Si} = 40\mathring{A}$ and $d_{ZnS} = 20\mathring{A}$ for (a) the first type and (b) the second type of the vibration modes.

14

V. Intersubband Scattering

Since the optical modes in the Si/ZnS superlattice consist of confined nonpolar Si and polar ZnS optical phonons, the calculation of carrier scattering by optical phonons in such a structure needs to include contributions from both types of phonons. The Hamiltonian that describes the carrier interaction with the nonpolar Si optical phonons is given by[30]

$$H = \frac{1}{2}\mathbf{D} \cdot \mathbf{u} \tag{39}$$

where $\mathbf{D}$ is the optical deformation potential. This Hamiltonian obviously vanishes outside of the Si layers in the Si/ZnS superlattice since the Si optical displacement modes are strictly confined within the Si layers. However, the carrier interaction with the confined polar ZnS optical phonons extends over both ZnS and Si layers. The electrical interaction Hamiltonian can be obtained using the scalar and vector potentials

$$H = -e\phi + \frac{e}{m}\mathbf{A} \cdot \mathbf{p}, \tag{40}$$

where $\mathbf{p}$ is the momentum operator, e and m are the free electron charge and mass, respectively. Although the scalar potential ϕ associated with the LO mode vanishes in Si layers, the $\mathbf{A} \cdot \mathbf{p}$ interaction exists in both layers since the vector potential associated with the interface modes in the ZnS layers as shown in Fig.4 propagates into the Si layers as well.

A. Scattering due to Si Phonons

The displacement patterns described in Eqs.(5-7) all contain an arbitrary constant for the mode amplitude which can be normalized by equating the energy of the vibration mode with that of a simple harmonic oscillator[16]

$$\chi^2 = \frac{S}{\Omega} \int_0^{d_{Si}} \mathbf{u}^* \cdot \mathbf{u} dz, \tag{41}$$

where S is the sample surface area (in (x,y) plane), Ω is the volume of the unit cell, and χ is the normal coordinator of the oscillator. The heavy-hole state can be characterized by $|\mathbf{k}, n>$ with the in-plane momentum $\mathbf{k}$ and subband index n. In the approximation of constant effective mass for heavy holes, the matrix element for the transition from state $|\mathbf{k}, n>$ to $|\mathbf{k}', n'>$ due to the emission of a nonpolar Si optical phonon is

$$<\mathbf{k}', n'|H|\mathbf{k}, n> = \begin{cases} \sqrt{\dfrac{\hbar[n(\omega_o) + 1]}{2\rho_{Si}\omega_o S d_{Si}\Delta_A(q_z)}}\delta_{\mathbf{k}'\pm\mathbf{q}_x,\mathbf{k}}D_y G_{nn'}^y(q_z) & \text{(s-TO)} \\ \sqrt{\dfrac{\hbar[n(\omega_o) + 1]}{2\rho_{Si}\omega_o S d_{Si}\Delta_C(q_L, q_T)}}\delta_{\mathbf{k}'\pm\mathbf{q}_x,\mathbf{k}} \\ \quad \cdot [D_x G_{nn'}^x(q_L, q_T) + D_z G_{nn'}^z(q_L, q_T)] & \text{(hybrid)}, \end{cases} \tag{42}$$

for the s-TO mode and the hybrid of the LO and p-TO mode, respectively. $n(\omega_o)$ is the number of Si optical phonons at thermal equilibrium, and ρ_{Si} is the density

of Si. The three components of the optical deformation potential, D_x, D_y, and D_z are assumed equal to $D_o = D/\sqrt{3}$ in the calculation, in view of the assumption of isotropy. The Kronecker symbol indicates the in-plane (x, y) momentum conservation. The normalization factors are given by

$$\Delta_A(q_z) = \frac{1}{d_{Si}} \int_0^{d_{Si}} u_y^* u_y dz \qquad \text{(s-TO)},$$
$$\Delta_C(q_L, q_T) = \frac{1}{d_{Si}} \int_0^{d_{Si}} (u_x^* u_x + u_z^* u_z) dz \qquad \text{(hybrid)}. \tag{43}$$

The $G_{nn'}$-functions contain envelope wavefunctions, ψ_n and ψ_n', from which interference effect can be obtained. Specifically,

$$G_{nn'}^y(q_z) = \int_0^{d_{Si}} \psi_n^* \psi_{n'} u_y dz, \tag{44}$$

for the s-TO mode, and

$$G_{nn'}^x(q_L, q_T) = \int_0^{d_{Si}} \psi_n^* \psi_{n'} u_x dz,$$
$$G_{nn'}^z(q_L, q_T) = \int_0^{d_{Si}} \psi_n^* \psi_{n'} u_z dz, \tag{45}$$

for the hybrid of LO and p-TO mode. The heavy-hole energy levels and envelope wavefunctions are obtained by the finite square well model for the superlattice with the heavy-hole band offset taken to be $1.5eV$[14].

Applying the Fermi golden rule, we obtain the scattering rate due to the emission of a nonpolar Si optical phonon,

$$W_{nn'} = \begin{cases} \dfrac{m_{hh}^*[n(\omega_o) + 1]D_o^2}{2\hbar^2 \rho_1 \omega_o d_{Si}} \sum_{q_x} \dfrac{|G_{nn'}^y|^2}{\Delta_A} & \text{(s-TO)} \\[3mm] \dfrac{m_{hh}^*[n(\omega_o) + 1]D_o^2}{2\hbar^2 \rho_1 \omega_o d_{Si}} \sum_{q_L, q_T} \dfrac{|G_{nn'}^x + G_{nn'}^z|^2}{\Delta_C} & \text{(hybrid)}, \end{cases} \tag{46}$$

where we have assumed that for the intersubband process $(n \neq n')$ the heavy holes are scattered from the bottom of their original subbands $(k = 0)$, and the sum is over those participating modes of Eq.(8) that, according to Eq.(4), yield values of q_x satisfying the in-plane momentum conservation[24].

B. Scattering due to ZnS Phonons

The normalization of the amplitudes of the confined ZnS displacement modes can be carried out by equating the energy of a hybrid, a mixture of mechanical and eletromagnetic energies, with that of a simple harmonic oscillator[16]. Since only the IP mode contributes electromagnetic energy which is small in magnitude when compared with the mechanical energy, neglecting it entirely will introduce little error in evaluating the energy of a hybrid ZnS mode. We therefore can use Eq.(41) for the normalization

16

of a ZnS mode, except that now the integral is over the ZnS layer, d_{ZnS}. The matrix element for the transition from state $|\mathbf{k}, n>$ to $|\mathbf{k}', n'>$ due to the emission of a polar ZnS optical phonon is

$$< \mathbf{k}', n'|H|\mathbf{k}, n >= \sqrt{\frac{e^2\hbar[n(\omega_{ZnS}) + 1]\omega_{ZnS}}{2Sd_{ZnS}\epsilon_P\Delta_{1,2}}}\delta_{\mathbf{k}'\pm\mathbf{q_x},\mathbf{k}}(-G_{nn'}^\phi + \frac{\hbar k_x}{m}G_{nn'}^x - \frac{i\hbar}{m}G_{nn'}^z) \quad (47)$$

for both the first and second types. $n(\omega_{ZnS})$ is the number of ZnS optical phonons at thermal equilibrium, and

$$\frac{1}{\epsilon_p} = \frac{1}{\epsilon_\infty} - \frac{1}{\epsilon_s}. \quad (48)$$

The normalization factors for both the first and second types can all be calculated by

$$\Delta_{1,2} = \frac{1}{d_{ZnS}}\int_0^{d_{ZnS}} (u_x^*u_x + u_z^*u_z)dz \quad (49)$$

with optical displacements given in Eqs.(22) and (23). The $G_{nn'}$-functions containing the interference effect between two subband envelope wavefunction, ψ_n and $\psi_{n'}$, are given specifically as

$$G_{nn'}^\phi = \frac{1}{\rho_o}\int_0^{d_{ZnS}} \phi\psi_n^*\psi_{n'}dz, \quad (50)$$

for the scalar potential scattering associated with the LO modes, and

$$G_{nn'}^x = \frac{1}{\rho_o}\int_0^{d_{ZnS}} A_x\psi_n^*\psi_{n'}dz,$$
$$G_{nn'}^z = \frac{1}{\rho_o}\int_0^{d_{ZnS}} A_z\psi_n^*\frac{\partial}{\partial z}\psi_{n'}dz, \quad (51)$$

for the vector potential scattering associated with the IP modes. Applying the Fermi golden rule, the intersubband scattering rate due to the emission of a polar ZnS phonon can then be obtained by taking summation over contributing confined ZnS optical modes

$$W_{nn'} = \frac{e^2m_{hh}^*[n(\omega_{LO}) + 1]\omega_{LO}}{2\hbar^2 d_{ZnS}\epsilon_p}\sum_{q_L}\frac{|-G_{nn'}^\phi + \frac{\hbar k_x}{m}G_{nn'}^x - \frac{i\hbar}{m}G_{nn'}^z|^2}{\Delta_{1,2}}, \quad (52)$$

where we have again assumed that the heavy holes are scattered from the bottom of subband n ($\mathbf{k} = 0$), and have taken the approximation of $\omega_{ZnS} = \omega_{LO}$ since the modes which interact most strongly with carriers are those with frequencies near the LO branch.

C. Intersubband Scattering Rates

The scattering rates due to the emission of Si and ZnS optical phonons were calculated for the intersuband transition (2-1) originated from the bottom of the heavy-hole subband 2 with zero kinetic energy to heavy-hole subband 1. Figure 6 shows the 2-1 scattering rates as a function of the Si well width while fixing the barrier width at

17

$d_{ZnS} = 40\mathring{A}$ in the Si/ZnS superlattice. The total scattering rate is the summation of contributions from the heavy-hole interaction with Si and ZnS optical phonons. In the small well width region ($d_{Si} < 30\mathring{A}$), the heavy-hole scattering due to the ZnS optical phonons is stronger than that due to the Si optical phonons. This is attributed to the fact that when the Si well width is small there is significant envelope function overlap between subbands 1 and 2 in the ZnS barrier region where the ZnS LO phonons are confined. As the well width increases, the distribution of envelope functions in the barrier decreases. As a result, the scattering due to the ZnS LO phonons reduces considerably and the ZnS phonon scattering is mostly through IP modes which propagate throughout the super-lattice structure. As the well width continues to increase, the energy separation between subband 1 and 2 decreases. The intersubband scattering between these two subbands requires an emitted ZnS phonon with a small in-plane wavevector (q_x) in order to satisfy the in-plane momentum conservation for the scattering process to take place. This leads to an increased intersubband scattering rate since polar optical phonons with smaller wavevectors interact more strongly with carriers to induce intersubband transitions as suggested by the well-known $1/(q_x^2 + q_z^2)$ dependence of the interaction Hamiltonian in polar material quantum wells[15]. A similar dependence of the intersubband scattering rate of Eq.(52) due to the confined ZnS optical phonons is implicitly included in the nor-malization factor ($\Delta_{1,2}$) given by Eq.(49). Further increasing the well width to $d_{Si} > 82\mathring{A}$ causes the energy separation between the two subbands to be less than the ZnS optical phonon energy ($43 meV$) and the heavy holes at the bottom of subband 2 cannot emit ZnS optical phonons to make a transition to subband 1, resulting in zero scattering rate due to the emission of ZnS optical phonon. The scattering rate due to the emission of Si optical phonon confined within the Si well demonstrates a steady decrease as the well width (d_{Si}) increases, which suggests that the factor $1/d_{Si}$ in Eq.(46) dominates the small increase in the interference effect $G_{nn'}$ function. As the well width increases beyond $62\mathring{A}$, the energy separation between the two heavy-hole subbands becomes less than the Si optical phonon energy ($64 meV$). As a result, the scattering rate due to the emission of Si optical phonons reduces to zero, in which case the heavy-hole lifetime of subband 2 can be enhanced dramatically since the significant scattering process of optical phonon emission is suppressed although the weaker optical phonon absorption and acoustic phonon scattering processes are still possible.

Figure 7 shows the intersubband scattering rates between the same two heavy-hole subbands due to the emission of both Si and ZnS optical phonons as a function of the barrier width (d_{ZnS}) in the Si/ZnS supperlattice. The well width (d_{Si}) is fixed at $30\mathring{A}$. The scattering rate due to the emission of Si optical phonons remains unchanged as the barrier width varies since the subband energy levels are hardly shifted and the $G_{nn'}$-function for the Si phonon scattering has little noticeable change. The scattering rate due to the emission of an ZnS optical phonon, on the other hand, demonstrates a decreasing trend as the ZnS barrier width increases as suggested in Eq.(52) with the factor of $1/d_{ZnS}$. The small discontinuous incremental steps in the ZnS-scattering curve are due to the discrete nature of the increase in the number of allowed LO modes confined
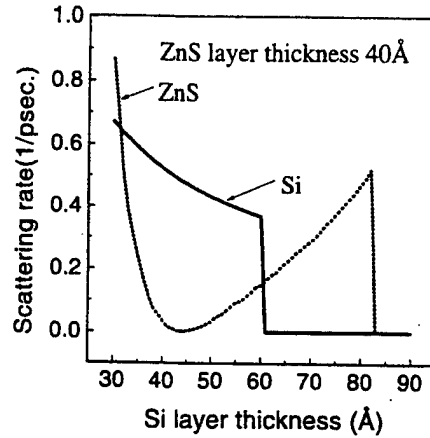
in the ZnS barrier as it increases.

Figure 6. Intersubband scattering rates due to the emission of Si and ZnS optical phonons as a function of Si well width (d_{Si}) for a barrier width of $d_{ZnS} = 40\mathring{A}$.
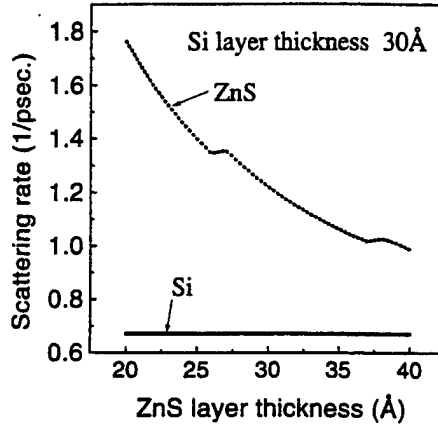

Figure 7. Intersubband scattering rates due to the emission of Si and ZnS optical phonons as a function of ZnS barrier width (d_{ZnS}) for a well width of $d_{Si} = 30\mathring{A}$.

VI. Summary and Discussion

We have provided an analytical model of optical modes in Si/ZnS superlattices consisting of polar and nonpolar optical phonons. This is a new procedure for obtaining the eigen modes of a mixed polar-nonpolar heterosystem. In the Si layers, a continuum model with double hybridization of the LO and TO modes is used to describe the vibration patterns. Since there is no electric field resulting from the nonpolar ionic displacements in Si layers, the only boundary condition that needs to be satisfied in the Si layers is the vanishing of the displacements at the Si-ZnS interface, as the ZnS layers can be considered as infinitely rigid with respect to the vibrations of the Si layer. Due to this strict confinement, only guided modes emerge in the Si layers which consist of s-TO

and coupled p-TO and LO modes, with no interface modes. These guided modes have been illustrated. Their interaction with carriers in the superlattice can be calculated through the optical deformation potential for Si. The interaction Hamiltonian can be obtained by taking the product of this potential with the normalized ionic displacement.

However, for the optical phonons in ZnS layers, we need to include the electrical interaction in calculating the carrier scattering by optical phonons, since there are electric fields associated with the polar optical vibrations. As a result, both mechanical and electrostatic boundary conditions need to be satisfied in the interfaces. A continuum model employing a linear combination of LO, TO and IP (interface polariton) modes with a common frequency is used to describe the ionic displacements in ZnS layers. A numerical procedure for determining a phonon frequency is provided. This hybridized model is necessary to meet the simultaneous requirement on the mechanical and electrostatic boundary conditions. The mechanical boundary condition is again the vanishing of the optical displacements since Si layers can be considered as infinitely rigid with respect to the vibrations of the ZnS layers. The electrostatic boundary conditions are the continuity of the electric field parallel to the interface, and the continuity of the displacement field normal to the interface. Based on this set of boundary conditions, expressions are obtained for the ionic displacements in ZnS layers consisting of LO, TO, and IP modes. There are scalar and vector potentials associated with the LO and IP modes, respectively, but no electric field associated with the TO mode. The scalar potential and its associated electric field due to the LO mode are distributed only within the ZnS layers and are zero in the Si layers. But the vector potential and its associated electric field due to the IP mode have distributions in both ZnS and Si layers even though there is no ZnS ionic displacement mode in the Si layers. Examples of these mode characteristics have been demonstrated. Neither the scalar nor vector potential is continuous across the Si-ZnS interface, but the energy of coherent interaction with carriers is continuous due to the continuity of the electric field parallel to the interface.

The analytical model for the confined optical modes consisting of polar and non-polar optical phonons is employed in calculating the carrier-phonon interaction. Our results indicate that contributions to heavy-hole intersubband scattering from confined Si and ZnS optical phonons strongly depend on the well width since it varies the distributions of envelope functions of involved subbands which ultimately determines the intersubband scattering between them through the overlapping interference effect $G_{nn'}$-function. For small Si well width ($< 30\mathring{A}$), the scattering rate due to ZnS optical phonon is stronger than that of Si optical phonons. As the well width increases the scattering rate due to the Si optical phonons surpasses that of ZnS optical phonons. The scattering rate dependence on barrier width is relatively weak.

References

[1] J. Faist, F. Capasso, D. L. Sivco, A. L. Hutchinson, C. Sirtory, and A. Y. Cho, Science **264**, 553 (1994)

[2] J. Faist, F. Capasso, D. L. Sivco, A. L. Hutchinson, C. Sirtory, S. N. G. Chu, and A. Y. Cho, Appl. Phys. Lett. **65**, 2091 (1994)

[3] G. Sun, L. Friedman, and R.A. Soref, Appl. Phys. Lett. **66**, 3425 (1995)

[4] R. A. Soref, Proc. IEEE **81**, 1687 (1993)

[5] L. Friedman and R. A. Soref, IEEE Photonics Technology Letters **5**, 1200 (1993)

[6] L. J. Schowalter and R. W. Fathauer, CRC Critical Review **15**, 367 (1989)

[7] R. Tsu, Nature **364**, 19 (1993)

[8] M Yokoyama, K. I. Kashiro, and S. I. Ohta, J. Crystal Growth **81**, 73 (1987)

[9] X. Zhou, S. Jiang, and W. P. Kirk, J. Appl. Phys. **82**, 2251-2262 (1997)

[10] E. G. Wang and C. S. Ting, Phys. Rev. B **51**, 9791 (1995)

[11] C. Maierhofer, S. Kulkarni, M. Alonso, T. Reich, and K. Horn, J. Vac. Sci. Technol. B **9**, 2238 (1991)

[12] M. Cardona and N. E. Christensen, J. Vac. Sci. Technol. B **6**, 1285 (1988)

[13] W. A. Harrison, J. Vac. Sci. Technol. **14**, 1016 (1977)

[14] S. Jiang, X. Zhou, T. Zhou, K. P. Clark, G. Spencer, R. T. Bate, W. P. Kirk, R. M. Steinhoff, and B. Brar, submitted to J. Appl. Phys. (Sept., 1997)

[15] B. K. Ridley, Phys. Rev. B **39**, 5282 (1989)

[16] B. K. Ridley, Phys. Rev. B **47**, 4592 (1993)

[17] M. P. Chamberlain, M Cardona, and B. K. Ridley, Phys. Rev. B **48**, 14356 (1993)

[18] N. C. Constantinou and B. K. Ridley, Phys. Rev. B **49**, 17065 (1994)

[19] B. K. Ridley, Appl. Phys. Lett. **66**, 3633 (1995)

[20] E. Molinari and A. Fasolino, Appl. Phys. Lett. **54**, 1220 (1989)

[21] L. register, Phys. Rev. B **45**, 8756 (1992)

[22] K. J. Nash, Phys. Rev. B **46**, 7723 (1992)

[23] N. Mori and T. Ando, Phys. Rev. B **40**, 6175 (1989)

[24] G. Sun and L. Friedman, Phys. Rev. B **53**, 3966 (1995)

[25] A. Fasolino, E. Molinari, and J. C. Mann, Phys. Rev. B **39**, 3923 (1989)

[26] B. K. Ridley, Phys. Rev. B **44**, 9002 (1991)

[27] S. C. Jain and W. Hayes, Semicond. Sci. Technol. **6**, 547 (1991)

[28] L. Friedman, R. A. Soref, and G. Sun, IEEE Photonics Technology Letters, **9**, 593 (1997)

[29] R. A. Soref, L. Friedman, L. C. Lew Yan Voon, L. R. Ram-Mohan, and G. Sun, submitted to J. Vac. Sci. Technol. B (Sept., 1997)

[30] B. K. Ridley, Quantum Processes in Semiconductors (Clarendon Press, Oxford, 1982), Chap. 3